EVOLUTIONARY BIOLOGY

# Conserved meiotic mechanisms in the cnidarian *Clytia hemisphaerica* revealed by *Spo11* knockout

**Catriona Munro[1,2], Hugo Cadis[1,2], Sophie Pagnotta[3], Evelyn Houliston[2], Jean-René Huynh[1]***



**During meiosis, DNA recombination allows the shuffling of genetic information between the maternal and paternal chromosomes. Recombination is initiated by double-strand breaks (DSBs) catalyzed by the conserved enzyme Spo11. How this crucial event is connected to other meiotic processes is unexpectedly variable depending on the species. Here, we knocked down *Spo11* by CRISPR in the jellyfish *Clytia hemisphaerica*. Germ cells in *Clytia Spo11* mutants fail to assemble synaptonemal complexes and chiasmata, and in consequence, homologous chromosome pairs in females remain unassociated during oocyte growth and meiotic divisions, creating aneuploid but fertilizable eggs that develop into viable larvae. *Clytia* thus shares an ancient eukaryotic dependence of synapsis and chromosome segregation on Spo11-generated DSBs. Phylogenetically, *Clytia* belongs to Cnidaria, the sister clade to Bilateria where classical animal model species are found, so these results provide fresh evolutionary perspectives on meiosis regulation.**

## INTRODUCTION

In meiosis, diploid germ cells undergo two rounds of nuclear division to produce haploid gametes. A crucial feature of meiosis is the pairing of maternal and paternal chromosome homologs during an extended prophase before segregating from each other on the first meiotic spindle (*1*, *2*). Their initial loose coupling is stabilized by the polymerization of a proteinaceous structure called the synaptonemal complex (SC), which holds together homologous axes and promotes genetic recombination (*3*). Exchanges between chromatids of homologous chromosomes, known as crossovers, result in the formation of physical links (chiasmata), which maintain homologs associated in pairs following depolymerization of the SC. Individual meiotic processes and the molecular actors at each step are generally well conserved among eukaryotes and likely descend from a common eukaryotic ancestor (*4*, *5*). Unexpectedly, however, functional studies in classical model organisms have revealed diversity in the chronology and interdependency of these early meiotic steps (*1*, *2*). This paradox has been highlighted by studies of Spo11, a meiosis-specific enzyme highly conserved across eukaryotes that is required for the formation of DNA double-strand breaks (DSBs) and the initiation of meiotic recombination (*6*–*15*). In many of the species studied, Spo11-generated DSBs are required for pairing and synapsis of the replicated homologous chromosomes, with crossover sites (chiasmata) required subsequently for maintaining the pairs until their correct segregation during meiotic divisions (*6*, *9*–*12*, *15*). There are, however, several exceptions, notably in the classical animal model species *Caenorhabditis elegans* and female *Drosophila melanogaster* (*7*, *8*, *16*). All animal models in which Spo11 function has been examined so far belong to the clade Bilateria (Fig. 1A). Cnidaria, which includes corals, anemones, and jellyfish, is the sister clade to Bilateria and offers a valuable evolutionary perspective on meiotic processes. The jellyfish *Clytia hemisphaerica* is now established as a cnidarian model species well suited for experimental manipulation, with simple organization and transparency of the gonads making them attractive for analyzing gametogenesis regulation in vivo (*17*, *18*). Furthermore, particularities of its life cycle (Fig. 1B) conveniently enable phenotypes of gene mutations targeted by CRISPR-Cas9 to be studied in clonally produced $F_0$ generation jellyfish, which bud from stable, vegetatively propagating polyp colonies (*19*).

## RESULTS

### Mapping early meiosis in *Clytia* jellyfish

To establish a framework for studies of early meiotic mechanisms in *Clytia*, we first documented the formation of the gonads in male and female jellyfish. Following their release from the polyp colony, baby jellyfish show four small patches of germline precursor cells, detectable by their enrichment in the protein and mRNA of Piwi (*20*), positioned midway along each radial canal at the sites of the future gonads (Fig. 1, C and D, and fig. S1, A and B). The gonads develop and expand as the jellyfish grows to sexual maturity, from about 1 mm to 1 cm in diameter over 2 to 3 weeks, remaining clearly visible within the transparent animal. They maintain a simple overall organization as germline cells proliferate and differentiate between two somatic tissue layers: the gastrodermis and the epidermis (Fig. 1C). In females, germ cells entering meiosis are detected by 4 to 5 days, when oocytes of all stages of prophase I can be identified (Fig. 1, C and E). Hoechst staining reveals classic figures of condensed chromatin during leptotene-zygotene and structured parallel tracks indicative of pairing and synapsis in pachytene (Fig. 1E). Diplotene nuclei show a distinctive Hoechst-negative "hole" with one or more diffuse Hoechst-positive patches appearing as the oocyte grows (Fig. 1E). Telomere fluorescence in situ hybridization (FISH) shows characteristic "bouquet" configurations in leptotene/zygotene oocytes (Fig. 1E). Diplotene-arrested oocytes undergo extensive growth to reach 180 to 200 μm in diameter. Fully grown oocytes become competent to undergo meiotic maturation and spawning, a process triggered daily in mature ovaries by a peptide hormone, maturation-inducing hormone (MIH), secreted in response to light (*21*–*23*). Following each spawning, "stage I"

[1]Center for Interdisciplinary Research in Biology (CIRB), College de France, CNRS, INSERM, Université PSL, Paris, France. [2]Sorbonne Université, CNRS, Laboratoire de Biologie du Développement de Villefranche-sur-mer (LBDV), Villefranche-sur-Mer 06230, France. [3]Centre Commun de Microscopie Appliquée, Université Nice Côte d'Azur, Parc Valrose, Nice 06108, France.
*Corresponding author. Email: jean-rene.huynh@college-de-france.fr

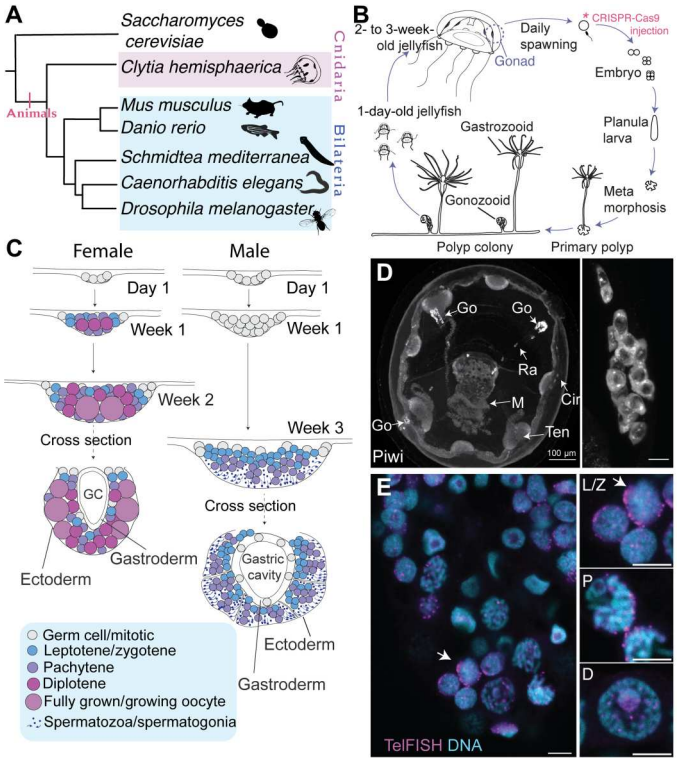


**Fig. 1. Phylogenetic placement, life cycle, and gonad organization of *C. hemisphaerica*.** (**A**) Evolutionary relationships among major animal meiosis models. Silhouettes from PhyloPic.org, *S. mediterranea*: credit to Noah Schlottman, *C. hemisphaerica*: credit to Joseph Ryan, photo by Patrick Steinmetz, under a share-alike license https://creativecommons.org/licenses/by-sa/3.0/. (**B**) Life cycle of *C. hemisphaerica*. The polyp colony propagates asexually for many years in the laboratory. Specialized polyps called gonozooids release jellyfish continuously. Sexually mature jellyfish release eggs or sperm daily in response to dark-light transitions. The embryo develops into a "planula" larva, which settles and metamorphoses to form a primary polyp. To achieve gene knockouts, CRISPR-Cas9 is injected in the mature egg immediately before fertilization. (**C**) Development and organization of the male and female gonad from the first day of jellyfish release to sexual maturity. GC, gastric cavity. (**D**) Maximum intensity projection of a confocal image stack of a 3-day-old jellyfish stained with anti-Piwi. Go, gonad; Ra, radial canal; M, manubrium/mouth; Ten, tentacle bulb; Cir, circular canal. Scale bar, 100 µm. A similar projection from a 3-day-old gonad is shown on the right. Scale bar, 10 µm. (**E**) Confocal section showing oocytes at mixed meiotic stages within the gonad of a 1-week-old female jellyfish stained with telomere FISH (magenta) and Hoechst (cyan). Scale bar, 10 µm. Inset shows close-up of representative nuclei at different prophase I stages; L/Z, leptotene/zygotene; P, pachytene; D, diplotene. Arrow indicates telomere bouquet. Scale bars, 5 µm.

growing oocytes of about 50 µm in diameter grow to full size in around 13 to 15 hours (*18*, *23*). Toward the end of this growth phase, the chromosomes condense in preparation for diakinesis (*18*). *Clytia* male jellyfish undergo a longer period of proliferation of germline precursors than females (Fig. 1C). After 2 weeks, prophase I spermatogonia are distributed in undulating layers, with leptotene/zygotene cells closest to the gastrodermis, then pachytene, spermatids, and, lastly, spermatozoa closest to the ectoderm (Fig. 1C and fig. S1, C and D). Daily sperm release occurs approximately 1.5 hours after light exposure. Within each subsequent 24-hour period, cohorts of spermatogonia enter and progress through pachytene, while in parallel, late pachytene cells enter diplotene and progress through the two meiotic divisions.

## Synapsis in *Clytia* is Spo11 dependent

We identified a single conserved *Clytia Spo11* gene using genome and transcriptome data (fig. S2) (*24*). We also identified other key meiosis SC components, such as Sycp1 and Sycp3, and the repair pathway proteins Rad51, Mlh1, and Dmc1 (fig. S3 and data S2 to S8). SC components are highly similar between cnidarians and many bilaterians, including mammals, while more divergence is observed among SC components from some other animal species, notably among ecdysozoans including *Drosophila* and *Caenorhabditis* (fig. S3) (*25*). Pachytene is characterized by a fully formed SC, which mediates tight association between each pair of duplicated chromosomes (*3*). We visualized meiotic progression and the SC in both males and females using antibodies generated to *Clytia* Sycp1, which forms the transverse filaments of the SC, and Sycp3, a component of the axial elements associated with each individual chromatid pair (Fig. 2). In wild-type female meiotic cells, Sycp3 is deposited along chromosome axes during zygotene, where it remains until diplotene; meanwhile, Sycp1 is present along chromosomes in short stretches during late zygotene and along the full length of chromosomes during pachytene, indicating that chromosomes are fully synapsed at the pachytene stage (Fig. 2A). Early and late stages of pachytene can be identified on the basis of the overall size of nuclei (Fig. 2A). Sycp1 is absent in diplotene, while Sycp3 is still present in early growth stages (Fig. 2A). In wild-type males, Sycp3 is deposited during leptotene/zygotene, while clear pachytene stages can be identified by Sycp1 across the full length of chromosomes during pachytene (Fig. 2, B to D).

We mutated the *Clytia Spo11* gene by injection into eggs of single CRISPR-Cas9 guide RNAs targeting either exon 1 or exon 2 (Fig. 3A and fig. S4). This generated $F_0$ male and female *Spo11* mutant polyp colonies, each containing small sets of insertion and deletion events around the targeted site but no detectable wild-type *Spo11* sequence (Table 1 and fig. S4). This typical outcome of CRISPR-Cas9 mutagenesis in *Clytia* reflects very active but inaccurate microhomology-mediated end joining repair of DSBs in the embryo, followed by reduction in genotypic complexity during larval metamorphosis (*19*). As expected, mutant alleles were invariant among jellyfish produced from the same mutant polyp colony.

We performed telomere FISH for two female *Spo11* mutants and could distinguish telomere bouquets characterizing leptotene/zygotene (fig. S5), indicating that interchromosomal interactions during these early stages are not dependent on Spo11 function. In *Spo11* mutants, we detected morphologically distinct pachytene-like stages with Sycp3 present along chromosome arms within both male and female gonads, but Sycp1 and thus SCs were absent in most pachytene nuclei, in rare cases, anti-Sycp1 decorating only occasional short chromosome stretches (Fig. 3B). Consistently, ladder-like SCs could be detected by electron microscopy in wild-type pachytene oocytes (Fig. 3C) but not in *Spo11* mutant pachytene oocytes (Fig. 3D and table S1). The earliest observable defect in *Clytia Spo11* mutants is thus a failure in synapsis, i.e., in the correct association of paired chromosomes via SC formation.

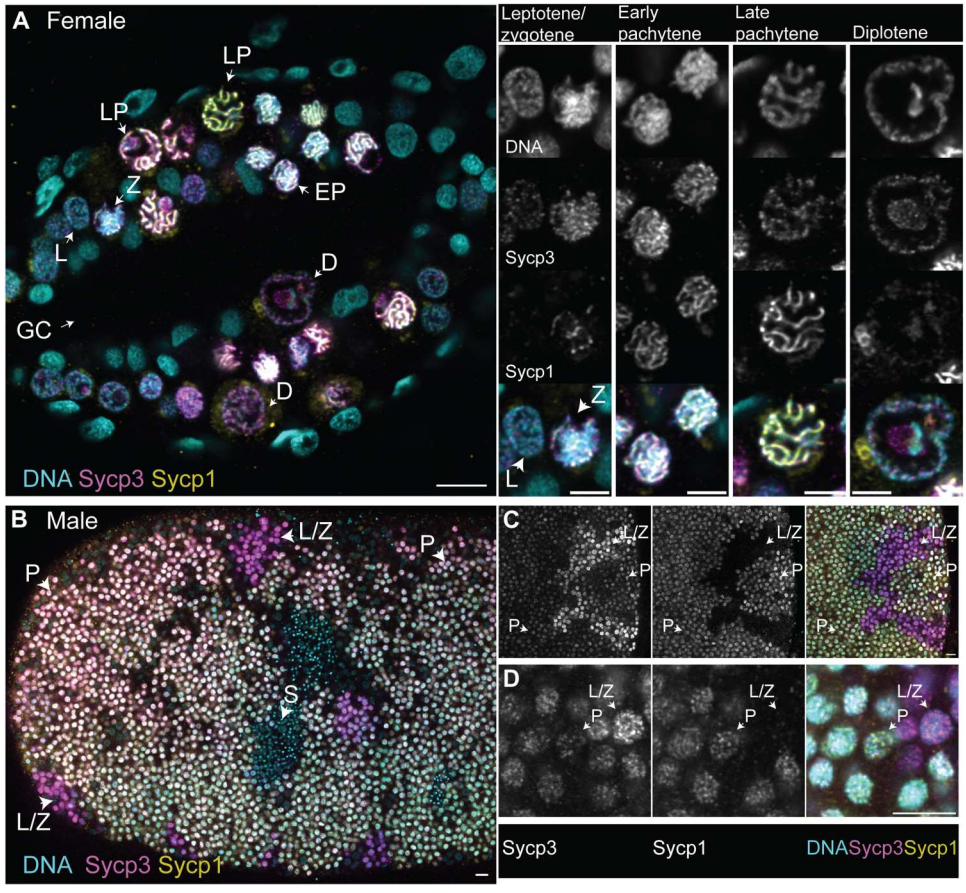


**Fig. 2. Meiotic progression in *Clytia* gonads.** Prophase I stages in females and males stained with anti-Sycp1 (yellow), anti-Sycp3 (magenta), and Hoechst dye (cyan). L, leptotene; Z, zygotene; P, pachytene; EP, early pachytene; LP, late pachytene; D, diplotene; GC, gastric cavity; S, spermatid/spermatozoa. (**A**) Confocal section of a 1-week-old female ovary. Scale bar, 10 μm; right inset is a close-up of representative prophase I stages. Scale bars, 5 μm. (**B**) Confocal section of a 3-week-old male gonad. Scale bar, 10 μm. (**C** and **D**) Zoom on the different confocal sections of a 3-week-old male gonad, highlighting leptotene/zygotene and pachytene stages. Scale bars, 10 μm.

## Chiasmata-mediated chromosome segregation fails in *Spo11* mutants

We predicted that in the absence of the SC, no crossover events would occur in *Spo11* mutants. A convenient feature of *Clytia* oogenesis for analyzing meiotic recombination events is that paired chromosomes connected at crossover sites can be readily detected within the enlarged nucleus ("germinal vesicle") of oocytes fixed and Hoechst-stained toward the end of the oocyte growth phase, as the chromatin transitions through a partially condensed state (Fig. 4A). From confocal z-stacks through the germinal vesicle of wild-type oocytes fixed at this stage, 15 pairs of chromosomes could be clearly distinguished in most cases, with one to two chiasmata detectable per pair (see Materials and Methods; mean chiasmata number, 1.76; median, 2; $n = 13$ oocytes; Fig. 4, B and C, top). In all female *Spo11* mutants, however, we consistently distinguished 30 scattered univalents at this stage, detecting no chiasmata ($n = 10$ oocytes; Fig. 4, B and C, bottom). This strong phenotype demonstrates that in *Clytia*, Spo11-mediated DSBs are necessary for crossovers and the formation of chiasmata, which, in turn, are required to maintain chromosome association during oocyte growth.

The loss of chiasma and the resulting scattering of individual duplicated chromosomes in fully grown oocytes had a severe impact on the subsequent meiotic divisions. When *Spo11* mutant oocytes are induced by MIH treatment to undergo meiotic maturation, univalents fail to align on a metaphase plate at the first division but rather remain distributed across defective spindle structures (Fig. 5, A and B, first column). No metaphase plates were observed on the spindles of *Spo11* mutant oocytes fixed during meiosis I (0 of 16 oocytes with anaphase/metaphase-type spindles identified), whereas in wild-type oocytes fixed at equivalent times, 17 clear metaphase plates and three anaphase figures were detected on 20 identified spindles. Moreover, polar body formation in *Spo11* mutant oocytes frequently aborts during anaphase I (Fig. 5, A and B, second column), such that in oocytes fixed after metaphase I, chromosomes were often found distributed into two or three patches (Fig. 5, A and B, third column, and Fig. 6C). As a consequence, meiosis II divisions are more varied, with zero, one, or sometimes two polar bodies appearing to form (21 of 23 fixed mutant oocytes show clear metaphase II defects; Fig. 5, A and B, third and fourth columns, and Fig. 6C).

Despite these severe abnormalities in the meiotic divisions, resulting typically in retention of two or four haploid sets of chromosomes in the oocyte (Fig. 5, D and E), *Spo11* mutant oocytes could be successfully fertilized with wild-type sperm at near wild-type frequencies. In most cases, the resulting zygotes developed into planula larvae and could undergo metamorphosis to the polyp

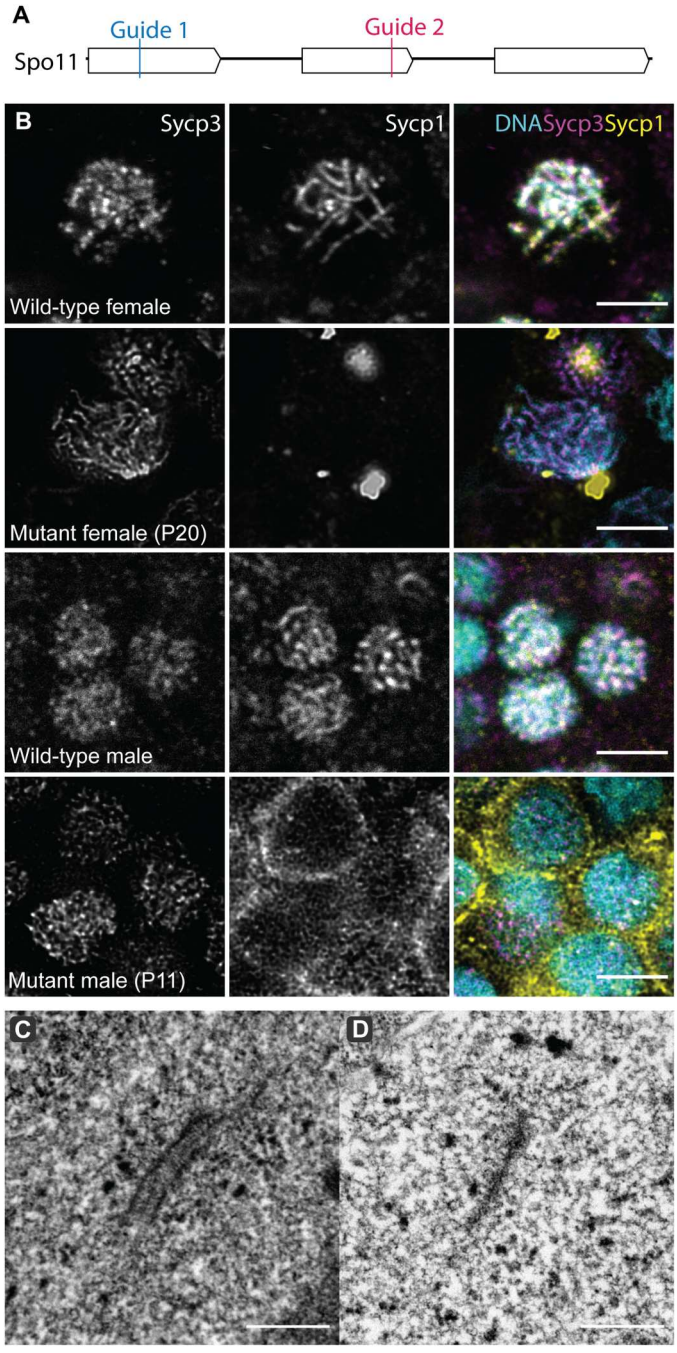


**Fig. 3. Spo11 is required for synapsis in *C. hemisphaerica* males and females.** (**A**) Diagram of the *Spo11* exons indicating the target sites of CRISPR-Cas9 guides. (**B**) Confocal planes of wild-type and *Spo11* mutant pachytene and pachytene-like nuclei stained with anti-Sycp1, anti-Sycp3, and Hoechst. Scale bars, 5 μm. (**C**). Transmission electron microscope (TEM) image of a wild-type SC. Scale bar, 0.5 μm. (**D**) TEM image of a *Spo11* mutant (P16) axial element. Counts are in table S1. Scale bar, 0.5 μm.

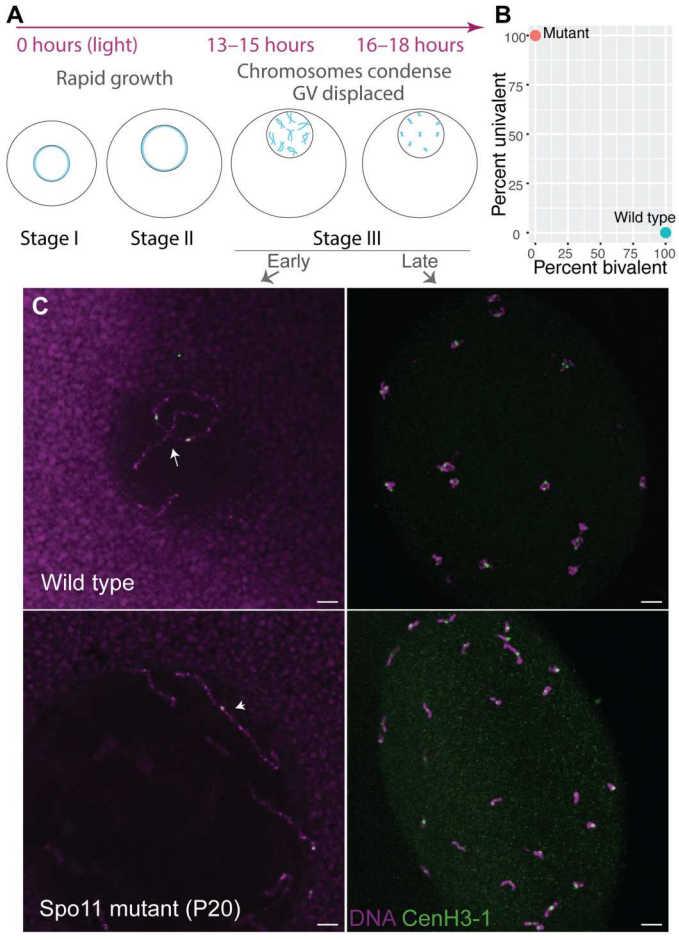


**Fig. 4. Spo11 is required for crossovers in *C. hemisphaerica*.** (**A**) Diagram of oocyte morphology during the 24 hours after spawning; stage I oocytes undergo rapid growth and displacement of the germinal vesicle (GV) and then, at stage III (fully grown), progressive condensation of chromosomes within the GV. (**B**) Percentage of univalent and bivalent chromosomes counted in *Spo11* mutant (P20 and P16) and wild-type fully grown oocytes ($n = 10$ oocytes). (**C**) Confocal images of stage III oocytes stained with Hoechst dye (purple) and anti–CenH3-1 (green). Left column images are of oocytes at an early stage of chromosome condensation (maximum projection of several z-stacks); right column images are of oocytes at a later stage of chromosome condensation (maximum intensity projections of z-stacks to show all chromosome pairs). Top left: Wild-type oocyte nucleus showing two homologous chromosomes with one chiasma (white arrow). Top right: Wild-type oocyte nucleus showing 15 pairs of chromosomes with one or two chiasma per pair. Bottom left: Mutant oocyte nucleus showing a single univalent (white arrowhead), with two other univalent arms in the top left and bottom right. Bottom right: Maximum intensity projection of a mutant oocyte nucleus showing 28 univalents and no bivalents (two chromatids likely obscured). Scale bars, 5 μm.

stage (table S2 and data S1). Metaphase chromosome spreads on 128/256-cell stage embryos confirmed that Spo11 mutant progeny are polyploid (Fig. 5, F and G). Similarly, Spo11 mutant males show no obvious loss of fertility, producing functional sperm capable of fertilizing wild-type oocytes to generate metamorphosis-competent larvae (table S2).

**Table 1. Summary of genotypes and phenotypes of Spo11 mutant colonies in this study.** N/A, not applicable.

| Colony name | Sex | Exon targeted | Most common alleles | Synaptonemal complex (Sycp1) | Chiasma in fully grown oocytes | Fertility |
|---|---|---|---|---|---|---|
| Q9 | Female | 1 | 5-bp deletion; 6-bp insertion | Absent* | No | Fertile |
| Q5 | Female | 1 | 6-bp insertion; 5-bp insertion; 5-bp deletion; 2-bp insertion | Absent* | No | Fertile |
| P20 | Female | 1 | 8-bp deletion; 4-bp deletion | Absent | No | Fertile |
| P16 | Female | 2 | 10-bp deletion; 184-bp deletion; 5-bp deletion/3-bp substitution | Absent | No | Fertile |
| P11 | Male | 1 | 1-bp deletion; large deletion/insertion | Absent | N/A | Fertile |

*Occasional partial SCs detected

## DISCUSSION

In this study, we show that meiosis in *C. hemisphaerica* relies on classical mechanisms of homologous chromosome synapsis, and the resulting chiasma is required to maintain homologous chromosomes associated during oocyte growth (Fig. 6). This sequence of meiotic events and their interdependencies revealed by Spo11 knockout in *Clytia* closely match those well described across eukaryotic model organisms, including mice, zebrafish, budding yeast, filamentous fungi, and plants, including *Arabidopsis thaliana* (*1*). They are thus likely governed by ancestral and conserved mechanisms.

Although Spo11-mediated DSBs are ultimately required for successful crossovers in all organisms examined, not all animal species share the same dependencies between the intervening events. Alternative modes of DSB-independent SC formation (synapsis) and pairing have notably been described in the traditional animal model species *C. elegans* and *D. melanogaster* (*7*, *8*). In males and females of *D. melanogaster*, chromosome pairing is unusual in initiating in proliferating germ cells before meiotic entry (*26*–*28*). This "prepairing" mode may have evolved to facilitate the marked specializations of gametogenesis in females and/or males in this species. In females, it could facilitate SC formation during the subsequent period of rapid oocyte differentiation, while in males, it could promote their particular SC-independent mechanism of chromosome pairing, which operates over an extended time window. *C. elegans* exhibits a distinct mode of recombination-independent chromosome pairing that occurs at "pairing centers," specialized sites at chromosome ends, and promotes the initiation of synapsis (*29*). It is likely that this involvement of pairing centers in synapsis evolved within the clade of *Caenorhabditis* since a classic role for Spo11 in chromosome pairing, synapsis, and crossover formation has been uncovered in another nematode species, *Pristionchus pacificus* (*15*). Another variation is seen in the planarian *Schmidtea mediterranea*, where pairing and synapsis do occur in spermatocytes but are not dependent on Spo11. It has been proposed that the telomere cluster plays a role in initiating SC formation, which, in turn, drives homolog pairing (*13*). Furthermore, homologous chromosomes in female silk moths (*Bombyx mori*) form SCs during meiosis but do not recombine, and a modified SC and telomeric pairing are suggested to play a role in keeping homologs together until anaphase I (*30*, *31*). The emerging picture from these studies, together with our findings, is that DSB formation was an important step toward synapsis in the common animal ancestor—a feature of meiosis shared with other sexual eukaryotes. While this persists today in *Clytia* and in vertebrates such as mice and fish, independent evolution of specialized gametogenesis programs in males and/or females of some other animal lineages appears to have diminished the importance of DSBs in initiating the SC. Thus, across animals, Spo11-mediated DSBs have remained essential for crossover formation and recombination but not for synapsis.

As a consequence of this highly conserved role for Spo11 in DSB-mediated crossing-over, Spo11 mutants across model species show defects in meiotic progression and/or chromosome segregation, as observed directly or implied by downstream effects on fertility. In mice, meiosis in *Spo11* mutants arrests in pachytene in males, while in females, oocytes progress through diplotene but are severely depleted within the ovary after birth (*9*, *10*). Similarly, spermatogenesis in *Spo11* mutant zebrafish arrests in early pachytene, and while females produce oocytes that can be fertilized, the vast majority of embryos show severe developmental defects and die before 5 days (*14*). *C. elegans Spo11* mutant hermaphrodites do produce fertilized eggs, but again, the vast majority die as embryos and display phenotypes indicative of meiotic segregation errors (*8*). In *D. melanogaster* females, *mei-W68* (*Spo11* homolog) mutants are fertile but display a strong nondisjunction phenotype (*7*, *16*). Likewise, outside of animals, in plants such as *A. thaliana* and fungi including *Saccharomyces cerevisiae*, *Sordaria macrospora*, and *Coprinus cinereus*, loss of *Spo11* leads to chromosome missegregation and reduced gamete or spore viability (*11*, *12*, *32*, *33*). The meiotic segregation defects that we have documented in *Clytia* thus mirror those reported for other species, confirming the importance of chiasmata for linking the two homologs and ensuring accurate homolog segregation during the first meiotic division (*34*, *35*). In marked contrast to other animal species, however, *Clytia* is unusually tolerant to aneuploidy (and more specifically, polyploidy) during development and metamorphosis. The consistently aneuploid *Clytia Spo11* mutant oocytes fertilize at normal rates and form polyploid embryos that can metamorphose. This finding opens up exciting possibilities to investigate in this species the behavior of aneuploid cells in $F_1$ individuals through mitosis and meiosis and the consequences of aneuploidy across generations.

Functional studies in phylogenetically distinct species provide invaluable insights into both conserved and divergent meiotic mechanisms. Along with practical advantages including

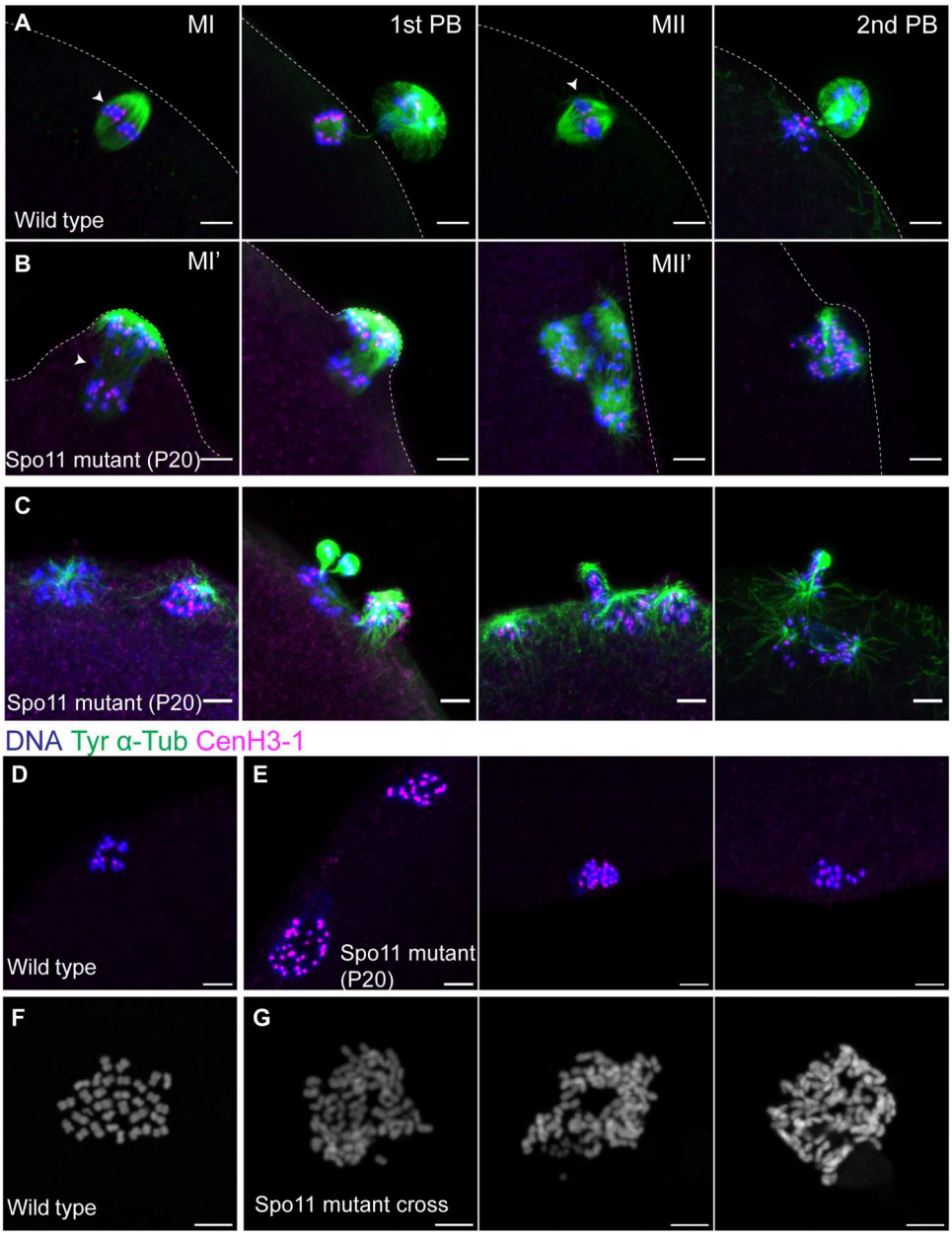


**Fig. 5. Meiotic division defects in Spo11 mutant oocytes.** DNA is stained with Hoechst dye (blue), microtubules are stained with anti–tyrosinated tubulin (green), and centromeres are stained with anti–CenH3-1 (magenta). Dotted lines contour the oocyte surface. (**A**) Wild-type meiotic divisions. From left to right: metaphase I (MI), first polar body (1st PB) emission, metaphase II (MII), and second polar body (2nd PB). White arrowheads indicate metaphase plates. Scale bars, 5 μm. (**B**) Spo11 mutant meiotic divisions. From left to right: metaphase I (MI'), white arrowhead indicates where the metaphase plate should be; failed emission of the first polar body; metaphase II (MII'); Spo11 mutant oocyte at the time of second polar body emission. Scale bars, 5 μm. (**C**) Examples of Spo11 mutants during meiosis II, following a failed emission of the first polar body. Scale bars, 5 μm. (**D**) Wild-type nucleus after meiosis is complete. DNA is stained with Hoechst dye (blue), and centromeres are stained with anti–CenH3-1 (magenta). Scale bar, 5 μm. (**E**) Three representative Spo11 mutant nuclei after meiosis are complete. DNA is stained with Hoechst dye (blue), and centromeres are stained with anti–CenH3-1 (magenta). Scale bars, 5 μm. (**F**) Metaphase spread of wild-type embryos stained with Hoechst dye. Scale bar, 5 μm. (**G**) Metaphase spreads of Spo11 mutant embryos stained with Hoechst dye. Scale bars, 5 μm.

transparent, simply organized gonads that are accessible to manipulation and observation, the jellyfish *C. hemisphaerica* offers a valuable evolutionary comparative perspective on meiotic mechanisms, which, in this model, are largely conserved from a distant eukaryotic ancestor.

## MATERIALS AND METHODS

Ethics approval is not required for experimentation on cnidarians.

### *C. hemisphaerica* cultures and maintenance

*C. hemisphaerica* cultures were maintained as described previously (*36*). Several wild-type strains were used in this study with

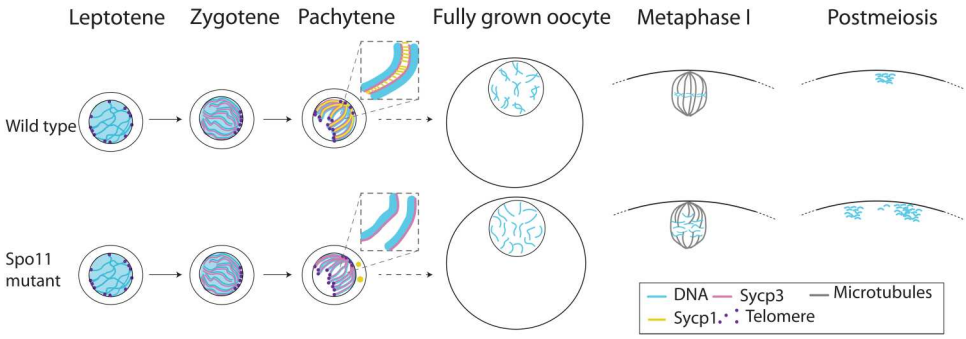


**Fig. 6. Summary of meiotic progression from leptotene to the first meiotic division and postmeiosis in wild-type and Spo11 mutants.** DNA (blue), Sycp3 (magenta/pink), Sycp1 (yellow), telomeres (purple), and microtubules (gray).

consistent results, including female strains Z11, Z4B, A2, Z21, Z28, and Z30 and male strains Z13, Z23, and A3. CRISPR-Cas9 mutant jellyfish were generated by injecting Z11 oocytes and fertilizing them with Z13 sperm, as well as Z30 oocytes with Z23 sperm.

### Gene identification and homology

*C. hemisphaerica* genes, for antibody, guide RNA, and FISH probe design, were identified via BLAST against the *Clytia* genome (http://marimba.obs-vlfr.fr/) (*24*). Gene alignments were made using MAFFT v7.453 L-INS-i (*37*), and gene phylogenies were generated with IQ-TREE (*38*) using an LG + F + R4 model. Gene trees and alignments are available in data S2 to S8.

### Spo11 CRISPR-Cas9 knockouts

Spo11 mutants were generated as described previously (*19*, *21*). Candidate guide RNAs with predicted cut sites between microhomologies were identified using http://rgenome.net/mich-calculator/, and off-target sites were identified using http://crispor.tefor.net/. Crispr RNA (crRNA) sequences are listed in table S3. Spo11 small guide RNA (sgRNA) was generated by hybridizing 200 μM crRNA and 200 μM trans-activating crispr RNA (tracrRNA) in the presence of 1× hybridization buffer (Integrated DNA Technologies, Coralville, IA), at 95°C for 5 min, and cooled to 25°C at −0.1°C/s. Two separate sgRNAs were injected, targeting regions of exon 1 and exon 2. Before injection, 0.5 μl of hybridized crRNA/tracrRNA (60 μM) was mixed with 2 μl of Cas9 protein (10 μM), incubated at room temperature for 10 min, adjusted with 0.84 μl of Cas9 buffer (10 mM Hepes and 350 mM KCl), and centrifuged at 14,000 rpm for 10 min at 12°C. Injection, fertilization, and subsequent metamorphosis of larvae were conducted as described previously (*19*, *21*).

### Genotyping

Genomic DNA was extracted from a single jellyfish using a DNeasy blood/tissue extraction kit (Qiagen). DNA around the target site was amplified using Phusion DNA polymerase (NEB, Ipswich, MA). Polymerase chain reaction (PCR) primer sequences are listed in table S3. PCR products were cleaned up and sequenced. Genotypes of *Clytia* mutant strains are in Table 1 and fig. S4.

### Antibodies

Antibodies recognizing *Clytia* Sycp1 were generated in rabbits using the two peptides IRNWKSEKEMELKMKD-Cys (75 to 90 amino acids) and Cys-PKAMTPKTPNMRYS (833 to 846 amino acids). Antibodies recognizing *Clytia* Sycp3 were generated in rats using the two peptides ENAPAEEAPAISGK-Cys (25 to 38 amino acids) and GRKRPAPHISHT-Cys (39 to 50 amino acids). Antibodies recognizing *Clytia* CenH3-1 were generated in mice using a recombinant protein generated in *Escherichia coli* against the full-length optimized sequence. Antibodies recognizing *Clytia* Piwi1 were raised in rabbits using a recombinant protein generated in *E. coli* against SGEPVQILTNYFKVDKMPRFEGLHQYVVAFDPDIQSQ KLKGFLLFSMQDVIGEVKVFDGMSLFLPRKLAEPVVERCVET RDGSSIKVKITHTNEVPVNSPQVVQLM (115 to 220 amino acids) fused with an N-his tag. All antibodies were generated and affinity-purified by Proteogenix (Schiltigheim, France).

For immunostaining, anti-Sycp1 antibodies were diluted 1:2000 for sycp1#4 and 1:1000 for sycp1#2. Sycp3#2 was diluted 1:400. For Sycp1 and Sycp3 double staining (two to three overnights), antibodies were diluted 1:4000 (sycp1#4) and 1:800 (Sycp3#2). Piwi#1 and Piwi#2 were diluted 1:2000. CenH3-1#2 was diluted 1:1000. Secondary antibodies (anti-mouse CenH3-1; anti-rabbit Sycp1, Piwi) were diluted 1:200. Rat monoclonal anti–tyrosinated tubulin YL1/2 was diluted 1:500 (Thermo Fisher Scientific, RRID: AB_2210201).

### Immunostaining

For anti-Sycp1 and anti-Sycp3 staining, samples (whole 1-week jellyfish or dissected gonads) were fixed in 1% formaldehyde in methanol at −20°C for at least 2 hours (up to overnight). Methanol fixed samples are left to warm gradually to room temperature (~30 min) before rehydration to phosphate-buffered saline (PBS). For anti-tubulin, anti–CenH3-1, and anti-Piwi1 staining, samples were fixed for 2 hours at room temperature in IF fix [0.1 M Hepes (pH 6.9), 50 mM EGTA (pH 7.2), 10 mM $MgSO_4$, 80 mM maltose, 0.2% Triton X-100, and 4% paraformaldehyde] for 2 hours before proceeding to washes and staining.

Anti-tubulin and anti–CenH3-1 staining included a methanol series: PBS-Triton 0.01%, three times for 10 min each; 50% methanol/50% PBS-0.1% Tween (PBST), once for 10 min on ice; 100% methanol, twice for 10 min on ice (or stored at −20°C after the second wash up to a week); and 50% methanol/50% PBST, once for 10 min at room temperature. All antibody staining then proceeded with the following washes (Triton X-100 used throughout): PBS-Triton 0.01%, three times for 10 min; PBS-Triton 0.2%, 40 min; PBS-Triton 0.01%, twice for 10 min; and PBS/bovine serum albumin (BSA) 3%, 20 min to 1 hour. Primary antibodies were diluted with PBS/BSA 3% and incubated with the sample at 4°C overnight. For Sycp1 and Sycp3 double staining, they were incubated over two to three nights. The next day, samples were washed

three times for 10 min with PBS-Triton 0.01%. Secondary antibody was diluted in PBS-Triton 0.01% and Hoechst 33342 1:5000, incubated with the sample for 2 hours at room temperature or overnight at 4°C, washed four times for 5 min with PBS-Triton 0.01%, and mounted in Citifluor antifade mountant (Citifluor-EMS).

### Telomere FISH

Telomere FISH was conducted using Cy3 and Alexa 647–labeled G-Rich telomere probe (Eurogentec, PN-TG020-005, PN-TG050-005) targeting repeats of TTAGGG. Probes were resuspended in formamide at 50 μM. A working aliquot was stored at 4°C for regular use, and the remaining aliquots were stored at −20°C for longer-term storage. Hybridization buffer solution was made fresh each time before starting the FISH protocol: 20 mM sodium phosphate $Na_2HPO_4$ (pH 7.4), 20 mM tris-HCl (pH 7.4), 60% deionized formamide, 2× SSC, 1× tRNA, and 1× Heparin.

FISH was conducted as follows: Samples [up to 1-week jellyfish (five to eight per tube), isolated oocytes] were fixed overnight at room temperature in HEM fix [0.1 M Hepes (pH 6.9), 50 mM EGTA (pH 7.2), 10 mM MgSO4, and 4% formaldehyde], washed three times for 10 min with PBST, and then dehydrated and rehydrated in methanol on ice (PBST/methanol 50%, once for 10 min; 100% methanol, twice for 10 min; PBST/methanol 50%, once for 10 min). Samples were then washed three times for 5 min with 2× SSC–0.1% Tween (pH 7). They were incubated in ribonuclease A solution (100 mg/ml) in an oven at 37°C for 1 hour. Then, they were washed three times for 5 min with 2× SSC–0.1% Tween (pH 7) at room temperature and then transferred to 50% hybridization buffer/2× SSC at 80°C for 5 min in a water bath. In parallel, the probe (1 μl in 99 μl of hybridization buffer) was heated to 90°C for 5 min. As quickly as possible, we removed as much as 50% hybridization buffer/2× SSC as possible and added the probe to the sample, gently flicking the tube to mix. The sample was then incubated for 10 min at 85°C in a water bath. Subsequently, samples were placed in the dark at room temperature for 1 hour for hybridization. After hybridization, samples were washed twice for 10 min with 2× SSC–0.1% Tween at 60°C in an oven (2× SSC–0.1% Tween was preheated to 60°C before washing). Samples were washed once with 2× SSC–0.1% Tween at room temperature, then stained with Hoechst dye 33342 1:5000 (30 min to 1 hour), washed three times for 5 min with 2× SSC, and mounted in Citifluor.

### In situ hybridization

In situ hybridization probes were produced as described previously (*39*), and in situ procedures were performed following the urea-based protocol (*40*).

### Confocal microscopy and quantification

Fluorescently labeled samples (FISH and immunohistochemistry) were imaged using Leica Stellaris 5, Sp8, or Sp5 laser scanning confocal microscopes. For each experiment, images of wild-type and mutant samples were collected using the same settings. All staining protocols were repeated for a minimum of three times. Crossover numbers were assessed by exploiting the partially condensed state of chromosomes in fully grown oocytes, easily visualized following Hoechst staining in fixed isolated oocytes. Chiasmata were identified by manual inspection of the z-stacks at instances where at least three strands of Hoechst-stained chromatin meet at a point. Chromosomes with orientations that did not enable clear identification of chiasmata were not included in the counts. Numbers of univalent and bivalent chromosomes in wild-type and mutant fully grown oocyte nuclei were determined similarly by manual counting of Hoechst-stained z-stacks of the entire volume of individual nuclei. Bivalents were defined by the presence of chiasmata between Hoechst-stained strands, and univalents were defined by the absence of detectable chiasmata.

### Transmission electron microscopy

For transmission electron microscopy, gonads were dissected from 4- and 5-day-old female jellyfish in 400 μM menthol in seawater (Sigma-Aldrich, #M2772, diluted from 1 M stock solution in ethanol). Fixation and embedding in epoxy resin were performed as described previously (*41*).

### Fertilization experiments

Embryos were generated as described previously (*36*) with the following crosses: mutant female x wild-type male and mutant male x wild-type female, with a control of wild-type female x wild-type male. Mutant or wild-type eggs were collected and added to glass dishes with the same volume of liquid. For female mutant crosses, the same volume of wild-type sperm was added to mutants as to wild type. If wild-type fertilization rate was low or development was disrupted, indicative of too much or too little sperm, results were discarded. In all experiments, adequate sperm concentration was verified by the presence of ~12 sperms around each egg. Raw counts are available in data S1.

### Meiotic maturation

Meiotic maturation was induced as described previously (*21*). Briefly, gonads were dissected from mutant and wild-type female jellyfish adapted to an afternoon light cycle and were maintained overnight in dishes with the light on. The following morning, fully grown oocytes were isolated, and MIH peptide (WPRPamide) was added to seawater containing the oocytes for a final concentration of 1000 nM. Oocytes were fixed every 5 min, starting 25 min after the addition of MIH.

### Metaphase spreads

Metaphase spreads were conducted on 128/256-cell stage embryos following the protocol of Guo *et al.* (*42*), with a few modifications: Nocodazole (Sigma-Aldrich) in dimethyl sulfoxide was used at a final concentration of 10 μM; embryos were treated in nocodazole for 1.5 hours at 18°C; embryos were washed in distilled water for 2.5 min; substantial pressure was applied to the coverslip.

## Supplementary Materials

**This PDF file includes:**
Figs. S1 to S5
Tables S1 to S3

**Other Supplementary Material for this manuscript includes the following:**
Data S1 to S8

## REFERENCES AND NOTES

1. D. Zickler, N. Kleckner, Recombination, pairing, and synapsis of homologs during meiosis. *Cold Spring Harb. Perspect. Biol.* **7**, a016626 (2015).
2. D. Zickler, N. Kleckner, A few of our favorite things: Pairing, the bouquet, crossover interference and evolution of meiosis. *Semin. Cell Dev. Biol.* **54**, 135–148 (2016).
3. S. L. Page, R. S. Hawley, The genetics and molecular biology of the synaptonemal complex. *Annu. Rev. Cell Dev. Biol.* **20**, 525–558 (2004).

4. U. Goodenough, J. Heitman, Origins of eukaryotic sexual reproduction. *Cold Spring Harb. Perspect. Biol.* **6**, a016154 (2014).
5. A. J. MacQueen, A. Hochwagen, Checkpoint mechanisms: The puppet masters of meiotic prophase. *Trends Cell Biol.* **21**, 393–400 (2011).
6. S. Keeney, C. N. Giroux, N. Kleckner, Meiosis-specific DNA double-strand breaks are catalyzed by Spo11, a member of a widely conserved protein family. *Cell* **88**, 375–384 (1997).
7. K. S. McKim, B. L. Green-Marroquin, J. J. Sekelsky, G. Chin, C. Steinberg, R. Khodosh, R. S. Hawley, Meiotic synapsis in the absence of recombination. *Science* **279**, 876–878 (1998).
8. A. F. Dernburg, K. McDonald, G. Moulder, R. Barstead, M. Dresser, A. M. Villeneuve, Meiotic recombination in *C. elegans* initiates by a conserved mechanism and is dispensable for homologous chromosome synapsis. *Cell* **94**, 387–398 (1998).
9. P. J. Romanienko, R. D. Camerini-Otero, The mouse Spo11 gene is required for meiotic chromosome synapsis. *Mol. Cell* **6**, 975–987 (2000).
10. F. Baudat, K. Manova, J. P. Yuen, M. Jasin, S. Keeney, Chromosome synapsis defects and sexually dimorphic meiotic progression in mice lacking Spo11. *Mol. Cell* **6**, 989–998 (2000).
11. M. Grelon, D. Vezon, G. Gendrot, G. Pelletier, *AtSPO11-1* is necessary for efficient meiotic recombination in plants. *EMBO J.* **20**, 589–600 (2001).
12. A. Storlazzi, S. Tessé, S. Gargano, F. James, N. Kleckner, D. Zickler, Meiotic double-strand breaks at the interface of chromosome movement, chromosome remodeling, and reductional division. *Genes Dev.* **17**, 2675–2687 (2003).
13. Y. Xiang, D. E. Miller, E. J. Ross, A. Sánchez Alvarado, R. S. Hawley, Synaptonemal complex extension from clustered telomeres mediates full-length chromosome pairing in *Schmidtea mediterranea*. *Proc. Natl. Acad. Sci. U.S.A.* **111**, E5159–E5168 (2014).
14. Y. P. Blokhina, A. D. Nguyen, B. W. Draper, S. M. Burgess, The telomere bouquet is a hub where meiotic double-strand breaks, synapsis, and stable homolog juxtaposition are coordinated in the zebrafish, Danio rerio. *PLOS Genet.* **15**, e1007730 (2019).
15. R. Rillo-Bohn, R. Adilardi, T. Mitros, B. Avşaroğlu, L. Stevens, S. Köhler, J. Bayes, C. Wang, S. Lin, K. A. Baskevitch, D. S. Rokhsar, A. F. Dernburg, Analysis of meiosis in *Pristionchus pacificus* reveals plasticity in homolog pairing and synapsis in the nematode lineage. *eLife* **10**, e70990 (2021).
16. K. S. McKim, A. Hayashi-Hagihara, *mei-W68* in *Drosophila melanogaster* encodes a Spo11 homolog: Evidence that the mechanism for initiating meiotic recombination is conserved. *Genes Dev.* **12**, 2932–2942 (1998).
17. E. Houliston, T. Momose, M. Manuel, Clytia hemisphaerica: A jellyfish cousin joins the laboratory. *Trends Genet.* **26**, 159–167 (2010).
18. C. Jessus, C. Munro, E. Houliston, Managing the oocyte meiotic arrest—Lessons from frogs and jellyfish. *Cells* **9**, 1150 (2020).
19. T. Momose, A. De Cian, K. Shiba, K. Inaba, C. Giovannangeli, J.-P. Concordet, High doses of CRISPR/Cas9 ribonucleoprotein efficiently induce gene knockout with low mosaicism in the hydrozoan *Clytia hemisphaerica* through microhomology-mediated deletion. *Sci. Rep.* **8**, 11734 (2018).
20. L. Leclère, M. Jager, C. Barreau, P. Chang, H. Le Guyader, M. Manuel, E. Houliston, Maternally localized germ plasm mRNAs and germ cell/stem cell formation in the cnidarian *Clytia*. *Dev. Biol.* **364**, 236–248 (2012).
21. G. Quiroga Artigas, P. Lapébie, L. Leclère, P. Bauknecht, J. Uveira, S. Chevalier, G. Jékely, T. Momose, E. Houliston, A G protein–coupled receptor mediates neuropeptide-induced oocyte maturation in the jellyfish *Clytia*. *PLOS Biol.* **18**, e3000614 (2020).
22. G. Quiroga Artigas, P. Lapébie, L. Leclère, N. Takeda, R. Deguchi, G. Jékely, T. Momose, E. Houliston, A gonad-expressed opsin mediates light-induced spawning in the jellyfish *Clytia*. *eLife* **7**, e29555 (2018).
23. A. Amiel, E. Houliston, Three distinct RNA localization mechanisms contribute to oocyte polarity establishment in the cnidarian *Clytia hemisphærica*. *Dev. Biol.* **327**, 191–203 (2009).
24. L. Leclère, C. Horin, S. Chevalier, P. Lapébie, P. Dru, S. Peron, M. Jager, T. Condamine, K. Pottin, S. Romano, J. Steger, C. Sinigaglia, C. Barreau, G. Quiroga Artigas, A. Ruggiero, C. Fourrage, J. E. M. Kraus, J. Poulain, J.-M. Aury, P. Wincker, E. Quéinnec, U. Technau, M. Manuel, T. Momose, E. Houliston, R. R. Copley, The genome of the jellyfish *Clytia hemisphaerica* and the evolution of the cnidarian life-cycle. *Nat. Ecol. Evol.* **3**, 801–810 (2019).
25. J. Fraune, M. Alsheimer, J.-N. Volff, K. Busch, S. Fraune, T. C. G. Bosch, R. Benavente, *Hydra* meiosis reveals unexpected conservation of structural synaptonemal complex proteins across metazoans. *Proc. Natl. Acad. Sci. U.S.A.* **109**, 16588–16593 (2012).
26. N. Christophorou, T. Rubin, J.-R. Huynh, Synaptonemal complex components promote centromere pairing in pre-meiotic germ cells. *PLOS Genet.* **9**, e1004012 (2013).
27. N. Christophorou, T. Rubin, I. Bonnet, T. Piolot, M. Arnaud, J.-R. Huynh, Microtubule-driven nuclear rotations promote meiotic chromosome dynamics. *Nat. Cell Biol.* **17**, 1388–1400 (2015).
28. T. Rubin, N. Macaisne, A. M. Vallés, C. Guilleman, I. Gaugué, L. Dal Toe, J.-R. Huynh, Pre-meiotic pairing of homologous chromosomes during Drosophila male meiosis. *Proc. Natl. Acad. Sci. U.S.A.* **119**, e2207660119 (2022).
29. A. J. MacQueen, C. M. Phillips, N. Bhalla, P. Weiser, A. M. Villeneuve, A. F. Dernburg, Chromosome sites play dual roles to establish homologous synapsis during meiosis in *C. elegans*. *Cell* **123**, 1037–1050 (2005).
30. S. W. Rasmussen, The transformation of the synaptonemal complex into the 'elimination chromatin' in Bombyx mori oocytes. *Chromosoma* **60**, 205–221 (1977).
31. L. F. Rosin, J. Gil Jr., I. A. Drinnenberg, E. P. Lei, Oligopaint DNA FISH reveals telomere-based meiotic pairing dynamics in the silkworm *Bombyx mori*. *PLOS Genet.* **17**, e1009700 (2021).
32. M. Celerin, S. T. Merino, J. E. Stone, A. M. Menzie, M. E. Zolan, Multiple roles of Spo11 in meiotic chromosome behavior. *EMBO J.* **19**, 2739–2750 (2000).
33. S. Klapholz, C. S. Waddell, R. E. Esposito, The role of the *SPO11* gene in meiotic recombination in yeast. *Genetics* **110**, 187–216 (1985).
34. A. T. C. Carpenter, Chiasma function. *Cell* **77**, 959–962 (1994).
35. M. Petronczki, M. F. Siomos, K. Nasmyth, Un Ménage à Quatre: The molecular biology of chromosome segregation in meiosis. *Cell* **112**, 423–440 (2003).
36. M. Lechable, A. Jan, A. Duchene, J. Uveira, B. Weissbourd, L. Gissat, S. Collet, L. Gilletta, S. Chevalier, L. Leclère, S. Peron, C. Barreau, R. Lasbleiz, E. Houliston, T. Momose, An improved whole life cycle culture protocol for the hydrozoan genetic model *Clytia hemisphaerica*. *Biol. Open.* **9**, bio051268 (2020).
37. K. Katoh, D. M. Standley, MAFFT Multiple sequence alignment software version 7: Improvements in performance and usability. *Mol. Biol. Evol.* **30**, 772–780 (2013).
38. B. Q. Minh, H. A. Schmidt, O. Chernomor, D. Schrempf, M. D. Woodhams, A. von Haeseler, R. Lanfear, IQ-TREE 2: New models and efficient methods for phylogenetic inference in the genomic era. *Mol. Biol. Evol.* **37**, 1530–1534 (2020).
39. P. Lapébie, A. Ruggiero, C. Barreau, S. Chevalier, P. Chang, P. Dru, E. Houliston, T. Momose, Differential responses to Wnt and PCP disruption predict expression and developmental function of conserved and novel genes in a cnidarian. *PLOS Genet.* **10**, e1004590 (2014).
40. C. Sinigaglia, D. Thiel, A. Hejnol, E. Houliston, L. Leclère, A safer, urea-based in situ hybridization method improves detection of gene expression in diverse animal species. *Dev. Biol.* **434**, 15–23 (2018).
41. E. A. Eisenman, M. Alfert, A new fixation procedure for preserving the ultrastructure of marine invertebrate tissues. *J. Microsc.* **125**, 117–120 (1982).
42. L. Guo, A. Accorsi, S. He, C. Guerrero-Hernández, S. Sivagnanam, S. McKinney, M. Gibson, A. Sánchez Alvarado, An adaptable chromosome preparation methodology for use in invertebrate research organisms. *BMC Biol.* **16**, 25 (2018).


**Acknowledgments:** We thank T. Momose for advice and help with CRISPR-Cas9 protocols and culture of mutant colonies, L. Rouressol for assisting with exploration of male *Clytia* gametogenesis, J. Uveira for assistance with P20 genotyping, R. Lasbleiz and A. Duchene at the Marine Resources Center (CRBM), and S. Schaub at the imaging platform (PIV) of Institut de la Mer de Villefranche. We thank the Huynh and Houliston/Momose laboratories for helpful comments on the manuscript. Transmission electron microscopy was performed at the Plateforme Commune de Microscopie Electronique, Université Côte d'Azur. **Funding:** The Marine Resources Center (CRBM) and PIV are supported by EMBRC-France, whose French state funds are managed by the ANR within the Investments of the Future program under reference ANR-10-INBS-02. This project received funding from the European Union's Horizon 2020 research and innovation programme under the Marie Skłodowska-Curie grant agreement no. 841433 (JOLI) to C.M. and J.-R.H., from the CNRS-INSB "Diversity of Biological Mechanisms" program to J.-R.H., and from the European Union's Horizon 2020 research and innovation programme no. 730984, ASSEMBLE Plus project, JRA3 to Sorbonne Université. The J.-R.H. laboratory is supported by CNRS, INSERM, Collège de France, La Fondation pour la Recherche Médicale (FRM) (Equipes FRM DEQ20160334884), Agence Nationale de la Recherche (ANR) (ANR-15-CE13-0001-01, AbsCyStem), and the Bettencourt Schueller Foundation. **Author contributions:** Conceptualization: J.-R.H., C.M., and E.H. Writing: C.M., J.-R.H., and E.H. Investigation: C.M., H.C., and S.P. Formal analysis: J.-R.H., E.H., and C.M. **Competing interests:** The authors declare that they have no competing interests. **Data and materials availability:** All data needed to evaluate the conclusions in the paper are present in the paper and/or the Supplementary Materials.

Submitted 1 June 2022
Accepted 22 December 2022
Published 27 January 2023
10.1126/sciadv.add2873